Analysis of Faraday effect in multimode tellurite glass optical fiber for magneto-optical sensing and monitoring applications

Analysis of Faraday effect in multimode tellurite glass optical fiber for magneto-optical sensing and monitoring applications

Yin Shiyu,[1] Joris Lousteau,[1] Massimo Olivero,[1] Marco Merlo,[1] Nadia Boetti,[1] Silvio Abrate,[2] Qiuling Chen,[1] Qiuping Chen,[1] and Daniel Milanese[1,*]

[1]Politecnico di Torino, Corso Duca degli Abruzzi 24, 10129 Torino, Italy

[2]Istituto Superiore Mario Boella, via Boggio 61, 10138 Torino, Italy

*Corresponding author: daniel.milanese@polito.it

Received 23 April 2012; accepted 23 May 2012;
posted 1 June 2012 (Doc. ID 167104); published 29 June 2012

The design and fabrication of a tellurite glass multimode optical fiber for magneto-optical applications are presented and discussed. The analysis of the polarization shows that an optical beam, linearly polarized at the fiber input, changes to elliptically polarized with an ellipticity of 1:4.5 after propagating down the fiber. However, the elliptical distribution remains unchanged with or without an applied magnetic field, demonstrating that no circular dichroism occurs within the fiber. The Verdet constant of the tellurite glass in the fiber is measured to be 28 ± 0.5 rad $\cdot$ $(T \cdot m)^{-1}$, diverging by less than 3% from the Verdet constant found on the same glass composition in bulk form. These results demonstrate the feasibility to develop reliable tellurite glass fibers by the preform drawing method for magneto-optical applications.

OCIS codes: 160.2750, 160.3820, 160.2290, 060.2280.

1. Introduction

Current technologies that exploit the Faraday effect to realize optical isolators and circulators, magnetic field sensors, and electrical current sensors rely either on ferrimagnetic crystalline materials such as Bi:YIG or on paramagnetic rare-earth ion-doped glasses [1,2].

In a number of applications, the use of a glass presents peculiar advantages such as the isotropy of its physical properties and the low cost of synthesis and preparation. Among these, the most interesting advantage consists in the possibility to shape the glass into an optical fiber through a simple and highly productive manufacturing process. The prospect of using all-fiber optical components, compact and immune to electrical interference, is of particular interest for the applications mentioned above.

Unlike its paramagnetic counterpart, the diamagnetic contribution to the Faraday effect is independent of the glass temperature. Although the magnitude of the effect is typically lower in purely diamagnetic glasses than in paramagnetic glasses, the stability and the range of operation are improved, thus producing a remarkable advantage in sensing and monitoring applications.

Thanks to the high polarizability of Te^{4+} ions and the high transparency from visible wavelengths up to the mid-IR, TeO_2-based glasses exhibit the required characteristics for the development of efficient diamagnetic magneto-optic fiber components. Depending on the exact glass composition, the typical Verdet constant for tellurite glasses at 633 nm is $V_d = 28$ rad $\cdot$ $(T \cdot m)^{-1}$ [3–6], nearly one order of magnitude higher than that of silica glass, for which $V_d = 3.9$ rad $\cdot$ $(T \cdot m)^{-1}$ typically [7].

In spite of these promising properties, up to now only one publication [6] has reported on the

1559-128X/12/194542-05$15.00/0

Table 1. Composition, Glass Transition Temperature (T_g), Crystallization Temperature (T_x), RI, and CTE for the TZN1 and TZN2 Tellurite Glass Compositions, Later Drawn as Core and Cladding of the Magneto-Optic Tellurite Fiber

Glass Name	Glass Composition (% mol)	T_g (°C) ±3	T_x (°C) ±5	RI at 633 nm ±0.001	CTE (K^{-1}) × 10^6 ±0.1
TZN1	$72TeO_2$:20ZnO:$8Na_2O$	294	405	2.016	16.3
TZN2	$70TeO_2$:20ZnO:$10Na_2O$	287	398	1.991	17.2

implementation and characterization of the Faraday effect in a tellurite glass fiber. The fiber used in [6] was developed by pressure-assisted filling of silica glass microcapillaries with tellurite glass. However, the value of the Verdet constant measured in this fiber was only half of the value measured in bulk material. A likely origin of such discrepancy is attributed to the thermal expansion mismatch between silica and tellurite glasses, which could induce sufficient stress to alter the refractive index (RI) of the tellurite glass and its spectral dispersion behavior. In terms of sensor design, such a discrepancy might be unacceptable, especially if the physical phenomena underneath are not fully understood and controlled. In this letter, following a different fabrication method, we report on the fabrication of a tellurite glass fiber and characterization of its magneto-optics properties and compare them with the properties of the corresponding tellurite bulk glass sample. Finally, we discuss engineering aspects related to the fiber fabrication and to its modal properties with the aim of increasing the magneto-optic sensitivity of the tellurite glass fiber.

2. Tellurite Fiber Fabrication and Optical Setup

For manufacturing the tellurite glass optical fiber, two tellurite glass compositions named TZN1 and TZN2 were synthesized as core and cladding, respectively. Their compositions are reported in Table 1, along with their glass transition temperatures T_g and RI, measured at 633 nm.

The glass compositions were designed to obtain matched thermomechanical properties and a fiber numerical aperture (NA) higher than the NA of the launching microscope objective (MO1) used to couple the light into the fiber (Fig. 1). As depicted in Table 1, the two glasses exhibit glass transition temperatures separated by only 7 K, and the coefficient of thermal expansion (CTE) differ by less than 5%. The difference of RI values between the two glass compositions provided a fiber NA of 0.32 at 633 nm.

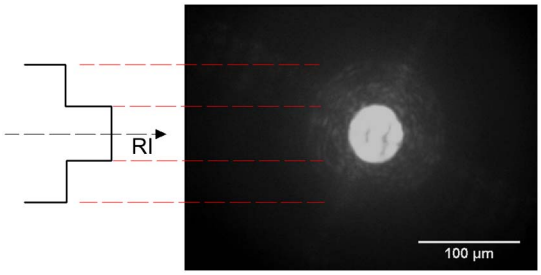

Fig. 1. (Color online) Photography of the output near field of the fiber when illuminated with a 1550 nm laser diode. RI profile of the fiber is also shown (inset) for illustrating the step index configuration of the fiber.

The fiber preform was fabricated using the rod-in-tube technique that is standardly used for the manufacturing of soft glass optical fibers [8]. A 10.6 mm outer diamer (OD) × 4.5 mm inner diameter (ID) tube made of TZN2 glass was made by rotational casting technique at 3000 rpm. A 10 mm diameter rod made of TZN1 glass was manufactured by melt quenching in a brass mold and then further stretched down to a diameter of 4.5 mm. After polishing using a 1 μm diamond paste organic solution, the rod and the tube were mounted in a fiber drawing tower. About 150 m of fiber were drawn, while an online monitoring system was tracking the fiber diameter. The fiber diameter along the entire spool was 138 ± 7 μm with an internal core of 56 ± 4 μm. A near-field imaging of the fiber, excited by a 1550 nm laser diode, is shown in the inset of Fig. 1. The fiber attenuation was measured by the cutback technique, and loss values of 3.5 dB/m and 2.6 dB/m were found at 980 and 1550 nm, respectively. Considering the high NA and the large core diameter, the fiber operates in the multimode regime at visible wavelengths. This was confirmed by near-field imaging at 633 nm, when the light of a He-Ne laser (Polytec, Germany) was coupled into the fiber and the modal distribution turned to be sensitive to the input coupling.

The fabrication of a smaller core tellurite glass fiber does not present a technical challenge. An additional step that consists in stretching the preform and then inserting it in a second cladding glass tube would allow for manufacturing a fiber with single-mode dimensions. Nevertheless, in this work a large-core fiber structure was selected for improving the optical power launching efficiency. In fact, the increased power propagating down the fiber facilitates the observations and the measurements of power variations induced by the Faraday effect through the optical setup described below.

After fabrication, a 0.7 m long straight section of tellurite glass fiber was mounted on the optical bench as shown in Fig. 2, using two magnetic clamps at the fiber tips. A He-Ne laser, emitting 1.8 mW in a linearly polarized laser beam about 1 mm in diameter, was focused on the fiber end-face using a × 10 microscope objective with NA = 0.28, resulting in a launching efficiency of 29%. The polarization extinction ratio of the laser beam was measured to be better than 1:5000. The fiber was surrounded by an in-house-made solenoid, consisting of a copper electrical wire, 2 mm in diameter, coiled into 180 turns around a 19 cm long PTFE tube with a radius of $r_1 = 11.5$ mm. The overall outer radius of the

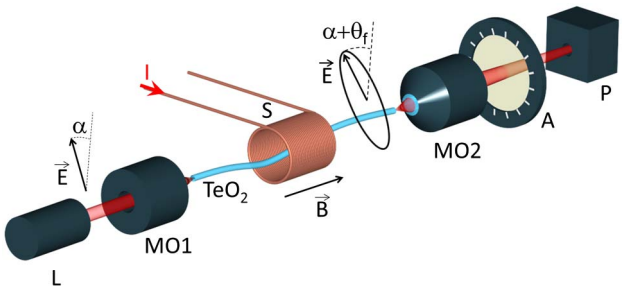

Fig. 2. (Color online) Experimental setup for characterizing Faraday effect in tellurite glass fiber manufactured in this work. L, polarized laser source at 633 nm; MO1, input microscope objective; TeO_2 fiber, tellurite glass optical fiber; S, copper wire solenoid; MO2, output microscope objective; A, polarization analyzer; P, photodetector.

electrical coil was $r_2 = 17$ mm. From the Biot–Savart law, the theoretical magnetic field density distribution along the tellurite glass fiber is given by Eq. (1):

$$B_{\text{th}}(x) = \frac{\mu \cdot I \cdot N}{2l(r_2 - r_1)} \left((x + l/2) \cdot \ln \frac{\sqrt{r_2^2 + (x + l/2)^2} + r_2}{\sqrt{r_1^2 + (x + l/2)^2} + r_1} - (x - l/2) \cdot \ln \frac{\sqrt{r_2^2 + (x - l/2)^2} + r_2}{\sqrt{r_1^2 + (x - l/2)^2} + r_1} \right). \quad (1)$$

The magnetic field density was measured, using a teslameter (PHYWE, 13610-93), at several positions along the solenoid, which was excited by a current of 1 A.

Finally, the experimental distribution was obtained by fitting experimental data B_{exp} against the linear equation $B_{\text{exp}} = \alpha_{\text{fit}} \cdot B_{\text{th}}$. Best fitting was obtained for $\alpha_{\text{fit}} = 0.981$. Theoretical and experimental magnetic field distributions are shown in Fig. 3.

As seen in Fig. 2, the beam propagates through the tellurite glass fiber and then passes through a polarizing filter, which was mounted on a rotational stage graduated with a precision of 3×10^{-4} rad and that acts as a polarization analyzer. The power of the output beam was then measured using a photodetector (Ophir PD300) having a dynamic range of 30 dB down to a power level of 0.02 nW.

3. Faraday Effect in Tellurite Glass Bulk and Fiber

A. Verdet Constant of Tellurite Glass Bulk

Prior to fiber characterization, a 3.8 mm thick bulk sample of glass TZN1 was synthesized and flat polished using a 1 μm diamond-paste organic solution. The Verdet constant, V_d, of this glass sample was measured following the procedure described by Davis and Bunch [9] under a permanent magnetic field.

This magnetic field was generated using a commercial solenoid better adapted to the shape of the glass bulk sample and to its short optical pathlength.

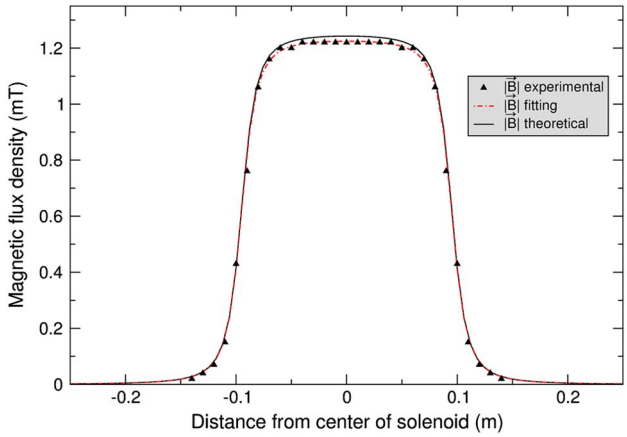

Fig. 3. (Color online) Magnetic field density with respect to position along the solenoid ($x = 0$ corresponds to central position of solenoid). B_{exp} corresponds to experimental data point, B_{th} arises from Eq. (2), and B_{fit} is the resulting curve of experimental data fitting against Eq. (2).

The solenoid consisted of two layers of 62 turns of 1 mm thick copper coiled around a 40 mm side, square frame-shaped beam. The sample was positioned at the center of the solenoid where a magnetic flux density value $B = 20$ mT was measured to be constant along the entire length of the bulk sample. A value of $V_d = 27.2 \pm 0.8$ rad·(T · m)$^{-1}$ was found for the bulk sample of glass TZN1, which is in good agreement with values reported in the literature for similar glass compositions [3–6].

In order to provide the reader with an overview of the potential of tellurite glass, Table 2 shows the Verdet constant of paramagnetic materials and the specific rotation of ferromagnetic materials standardly used for magneto-optical applications. Table 2 also shows the figure of merit (FOM) $= \rho_F/\alpha$ as used in [1,6], where ρ_F is the specific rotation in rad and α the absorption coefficient in cm^{-1} of the material

Table 2. Overview of Magneto-Optic Material Properties of Tellurite Glass as Compared to Those of Paramagnetic and Ferromagnetic Materials Standardly Used for Magneto-Optic Applications [1,6]

Material	V_d (rad T^{-1} m^{-1}) at $\lambda = 633$ nm	ρ_F (rad m^{-1})	FOM (ρ_F/α) (rad)
Tellurite glass[a]	27.2[b]	0.272[b]	2.5[b] 2.7[e]
Flint glass[a]	9.23[b]	0.093[b]	NA
Tb^{3+} doped SiO_2-based glass[a]	62.8[b]	0.63[b]	2.2[a] 0.7[c]
$Tb_3Ga_5O_{12}$[a]	134[b] 40[c]	1.34[b] 0.4[c]	 5[c]
Bi:YIG	NA	2180[d]	46[d]

[a]For diamagnetic and paramagnetic materials, the specific rotation was arbitrarily calculated for an applied magnetic flux density of 10 mT. Data are taken from [1,6].
[b]Measurements performed at a wavelength $\lambda = 633$ nm.
[c]Measurements performed at $\lambda = 950$ nm.
[d]Measurements performed at $\lambda = 1$ μm.
[e]Measurements performed at $\lambda = 1.5$ μm.

at the wavelengths considered. In the case of diamagnetic and paramagnetic materials, ρ_F was evaluated for an arbitrary magnetic flux density of 10 mT.

Several other parameters such as device application, device configuration, and measurement scheme should also be taken into account to identify the most appropriate material for a specific exploitation of the Faraday effect. Such considerations are out of the scope of the present article, where the purpose of Table 2 is to illustrate the characteristics of tellurite glass only.

As one can see, tellurite glass displays a Verdet constant of the same order of magnitude as paramagnetic glasses and crystals doped with rare-earth ions such as Tb^{3+}. However, unlike its paramagnetic counterparts, the FOM of tellurite glasses is independent of both temperature and wavelength. These features thus make tellurite glasses particularly attractive for the development of optical sensors. Despite the temperature dependence of their magneto-optic properties, ferromagnetic ceramics such as Bi-YIG remain materials of choice for most magneto-optics applications. However, synthesis and device manufacturing processes from these materials remain costly if compared to those used for the fabrication of tellurite glass fibers.

B. Polarization State of Fiber Output Beam

In order to evaluate the state of polarization of the beam at the fiber output, the optical power incident on the photodetector was measured at various angular positions of the analyzing polarization filter. These measurements were performed for two values of electrical current passing through the solenoid, $I = 0$ A and $I = 12$ A. Mechanical vibrations and thermal variations impaired the launching conditions as well as the output polarization state and mode coupling within the fiber, so that typical power fluctuations of −20 dB were observed during the measurements.

The two angular power distributions are shown in Fig. 4. In both cases, although initially linearly polarized, the optical beam has become elliptically polarized after propagating through the fiber with an ellipticity of the order of 1∶4.5. Possible sources of this change in polarization are residual birefringence in fiber [10], coupling between modes of different polarization state due to fiber defects [10], and stress-induced birefringence due to the fiber clamps. An elliptical power distribution was also found for a commercial silica-glass-based optical fiber having a 50 μm core, which served as a reference but for which an ellipticity value of 1∶7 was measured. The main difference between the tellurite glass fiber and the commercial silica fiber resides in the number of punctual defects and diameter fluctuations distributed along the tellurite fiber. The difference in ellipticity values between the two types of fibers suggests thus that fiber defects play an important role in the polarization change occurring within the tellurite fiber. Nonetheless, the direction of the main axis of the

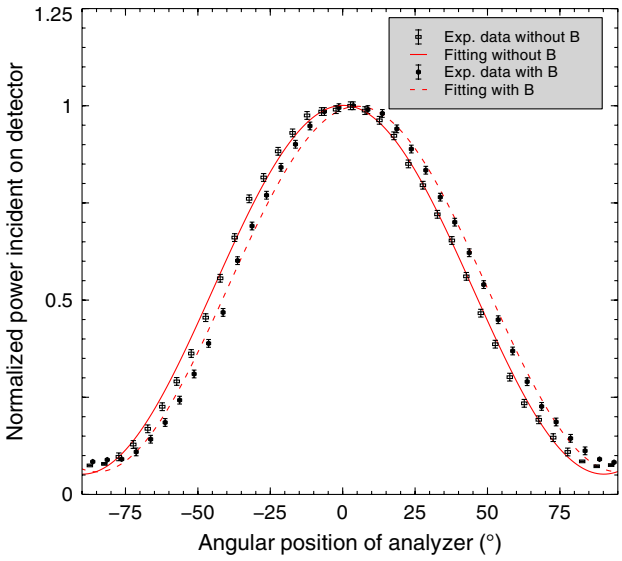

Fig. 4. (Color online) Distributions of fiber output power incident on photodetector versus $(\theta - \alpha)$, which is the angular position of the analyzer with respect to input linear polarization. Distributions obtained without magnetic field applied ($I = 0$ A through solenoid) and with magnetic field applied ($I = 12$ A passing through solenoid).

elliptical polarization at the fiber output corresponds to the direction of the linear polarization of the input launched beam. The polarization direction tends thus to be conserved along the 0.7 m long tellurite fiber despite the highly multimode behavior of the tellurite glass fiber and the nonnegligible number of defects.

Moreover, with or without the magnetic field, the angular distributions of power shown in Fig. 4 exhibit the same ellipticity. This observation suggests that, unlike the fiber prepared by pump filling [6], no magnetic circular dichroism occurs in our tellurite glass fiber that has been prepared by preform drawing.

C. Verdet Constant Measurement of Tellurite Glass in Fiber Form

The Verdet constant of the tellurite glass in fiber form was measured as follows. The fiber output power P_0 was measured without magnetic field for an angular position θ of the analyzer. A magnetic field was then generated by passing an electrical current through the solenoid and the analyzer rotated until power reached the initial value P_0. The angular value difference between the two positions of the analyzer is equal to the Faraday rotation angle θ_f. A series of measurements were performed for several electrical current intensity values. The measured values of the Faraday rotation angle are reported in Fig. 5. For highest sensitivity under elliptically polarized light, such measurements were carried out for an initial angle of $\theta = \pi/4$ where $dP/d\theta$ is maximum.

The Verdet constant was calculated by fitting experimental data against the following equation:

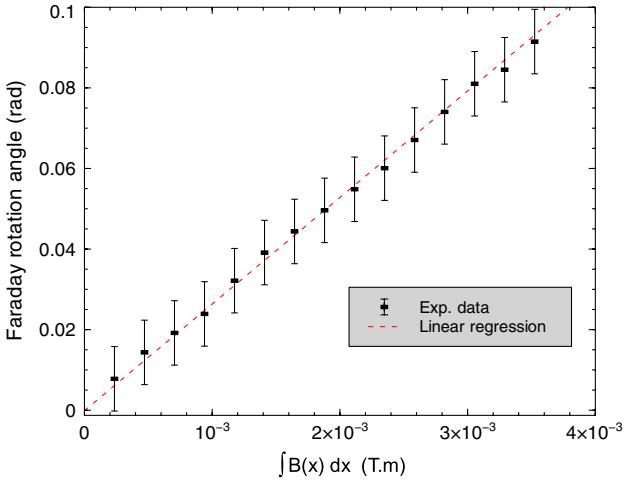

Fig. 5. (Color online) Faraday angle versus magnetic field density distribution along the tellurite fiber length. Experimental data and linear regression fitting are shown.

$$\theta_f = V_D \int_{-l/2}^{+l/2} B_{\text{fit}}(x)\mathrm{d}x, \tag{2}$$

where $l = 0.7$ m is the tellurite glass fiber length.

In order to validate our experimental setup and our methodology, the Verdet constant of a 50 μm core silica-based glass fiber was measured to be 4.0 ± 0.8 rad $\cdot$ $(\mathrm{T} \cdot \mathrm{m})^{-1}$. Although a nominal value is not available from the datasheet of the fiber manufacturer, the measurement result agrees with reported values of Verdet constant of silica-based glass measured in optical fiber [11–14].

The Verdet constant of tellurite glass TZN1 was found to be 28.1 ± 0.5 rad $\cdot$ $(\mathrm{T} \cdot \mathrm{m})^{-1}$. Taking into account error on measurements, this value can be considered equal to that found for the corresponding bulk material. This result suggests that the fiber drawing process did not affect the tellurite glass magneto-optical properties to a level sufficiently high to be detected by the optical setup presented in this letter.

Assuming further improvements on power stability with regards to mechanical vibrations, the simple setup described in this letter has the potential for measuring magnetic field variations as low as 4×10^{-5} T over a 20 cm long optical fiber. Further improvements on the fiber quality and packaging would also help maintaining a higher ellipticity ratio of the output polarization, hence increasing the sensitivity of the overall system.

4. Conclusion

Unlike the fiber fabrication procedure presented in [6], the manufacture of fiber via a simple preform drawing approach allows for preserving the magneto-optic properties of tellurite glasses from bulk to waveguide configuration. Although possible variations not detectable by our measurement setup are not excluded, the Verdet constants found for tellurite glass in bulk and fiber geometry have been measured to differ by less than 3% from one another. Furthermore, no extrinsic dichroism could be observed. The conservation of physical properties through the fiber manufacturing process should allow the reliable design of low-cost magneto-optical sensors based on diamagnetic tellurite glass fibers. In terms of possible configurations, polarization-maintaining or single-polarization fiber structures that lift polarization degeneracy might improve stability of operation, in particular by limiting the mode coupling effect. Nonetheless, the observation of the Faraday effect in a highly multimode fiber under suitable conditions of operation suggests the possibility to use large-core fiber in which high power can be launched, hence loosening the tight specifications on the detection systems in terms of noise level and responsivity.

The authors acknowledge the support of Regione Piemonte through the Converging Technologies "Hipernano" research project and of SAET GROUP (Leinì, Italy) for the induction heating system of the fiber drawing tower.

References

1. J. M. Liu, *Photonic Devices* (Cambridge University, 2005), Chap. 7.
2. M. Yamane and Y. Asahara, *Glasses for Photonics* (Cambridge University, 2000), Chap. 5.
3. N. F. Borrelli, "Faraday rotation in glass," J. Chem. Phys. **41**, 3289–3293 (1964).
4. A. Balbin Villaverde and E. C. C. Vasconcellos, "Magnetooptical dispersion of Hoya glasses: AOT-5, AOT-44B, and FR-5," Appl. Opt. **21**, 1347–1348 (1982).
5. I. A. Grishin, V. A. Gur'ev, E. B. Intyushin, E. E. Yu, O. V. Pavlova, and A. P. Savikin, "Magneto-optic and luminescent properties of tellurite glass TeO2-ZnCl2 doped with rare-earth elements," Russ. J. Appl. Chem. **77**, 1245–1248 (2004).
6. M. A. Schmidt, L. Wondrascek, W. L. Ho, N. Granzow, N. Da, and P. St. J. Russell, "Complex Faraday rotation in microstructured magneto-optical fiber waveguides," Adv. Mater. **23**, 2681–2688 (2011).
7. C. Z. Tan and J. Amdt, "Faraday effect in silica glasses," Physica B **233**, 1–7 (1997).
8. T. J. Miller and F. T. Geyling, "One-dimensional models for the co-drawing of preform rods in tubes," J. Lightwave Technol. **2**, 349–354 (1984).
9. J. A. Davis and R. M. Bunch, "Temperature dependence of the Faraday rotation of Hoya FR-5 glass," Appl. Opt. **23**, 633–636 (1984).
10. F. Tian, "Analysis of polarization fluctuation in single-mode optical fibers with continuous random coupling," J. Lightwave Technol. **34**, 1165–1168 (1987).
11. A. M. Smith, "Polarization and magnetooptic properties of single-mode optical fiber," Appl. Opt. **17**, 52–56 (1978).
12. S. C. Rashleigh and R. Ulrich, "Magneto-optic current sensing with birefringent fibers," Appl. Phys. Lett. **34**, 768–770 (1979).
13. R. H. Stolen and E. H. Turner, "Faraday rotation in highly birefringent optical fibers," Appl. Opt. **19**, 842–845 (1980).
14. J. L. Cruz, M. V. Andres, and M. A. Hernandez, "Faraday effect in standard optical fibers: dispersion of the effective Verdet constant," Appl. Opt. **35**, 922–927 (1996).